Journal of Cleaner Production 211 (2019) 1065–1077

Contents lists available at ScienceDirect

Journal of Cleaner Production

journal homepage: www.elsevier.com/locate/jclepro

Multi-fiber reinforced ettringite-based composites from industrial side streams

Hoang Nguyen [a], Malena Staudacher [b], Paivo Kinnunen [a], Valter Carvelli [c], Mirja Illikainen [a, *]

[a] Fibre and Particle Engineering Research Unit, University of Oulu, Pentti Kaiteran katu 1, 90014, Oulu, Finland
[b] Institute of Mechanical Process Engineering and Mineral Processing, Technical University Bergakademie Freiberg, Agricolastraße 1, 09599, Freiberg, Germany
[c] Department A.B.C., Politecnico di Milano, Piazza Leonardo Da Vinci 32, 20133, Milan, Italy

ARTICLE INFO

Article history:
Received 25 July 2018
Received in revised form
22 October 2018
Accepted 25 November 2018
Available online 26 November 2018

Keywords:
Fiber reinforced ettringite-based composite
Ladle furnace slag
Fly ash
Recycling
Sustainability
CO_2 emission

ABSTRACT

The development of high-performance cementitious composites from industrial side streams, which has both economic and environmental benefits, is of high demand. Ladle slag is a promising by-product from the steelmaking industry, which can form an ettringite-based binder. This experimental investigation focuses on the mechanical properties of different hybrid and mono fibers reinforced by ettringite-based binders from the ladle slag. The experimental results reveal that fibers greatly enhance the mechanical properties of the developed mixtures. The composites exhibit strain-hardening behavior with multiple cracks under flexural and tensile loading. In addition, the compressive strength of the composites can be 130% higher than the plain materials. To attain a balance between mechanical and economic aspects, a multi-criteria ranking method was used to evaluate 12 different mixtures. The ranking method suggests that a polypropylene micro fiber reinforced composite is the best mixture. The study recommends the efficient use of this industrial by-product for valuable applications in the construction industry.

© 2018 The Authors. Published by Elsevier Ltd. This is an open access article under the CC BY-NC-ND license (http://creativecommons.org/licenses/by-nc-nd/4.0/).

1. Introduction

In recent years, alternative cementitious materials from industrial side streams have been intensively studied to see if they can partly replace ordinary Portland cement (OPC) (Juenger et al., 2011; Luukkonen et al., 2018; Provis, 2017). Geopolymers and alkali-activated materials (AAMs) were identified as an eco-friendly candidate, since the materials offer up to 80% lower CO_2 emission than OPC (Duxson et al., 2007; van Deventer et al., 2010). However, this is not always the case; the cost and greenhouse gas emission of AAMs can be 39% and 14%, respectively, higher than that of conventional OPC concretes depending on the raw materials and transportation costs (McLellan et al., 2011). Another drawback of AAMs is the expense of obtaining alkali activators, including costs related to mining, transportation, and processing of raw materials. Hence, Passuello et al. (2017) suggested further studies of alternative alkali activators to achieve better environmental benefits for AAMs. Consequently, an inorganic binder with few activator chemicals used is of interest.

Ladle slag (LS), an industrial by-product from steel manufacturing processes, has been found to be a promising precursor for cementitious materials. Adesanya et al. (2017) developed alkali-activated LS with good mechanical properties (a compressive strength of roughly 56 MPa) and durability (a residual compressive strength of 49 MPa after 60 freeze-thaw cycles). Nguyen et al. (2018) produced high-performance polypropylene (PP) fibers reinforced alkali-activated LS with pseudo strain-hardening behavior (PSH)—that is, strain hardening behavior of brittle matrix attained by fibrous reinforcement. Furthermore, an ettringite-based binder was developed from the hydration between LS and gypsum (LSG) (Nguyen et al., 2019). This LSG material is a side-stream-based binder in which 98% of the raw materials can be from non-virgin materials, with minor citric acid amount as a retarder. Instead of landfilling or using LS in low-valuable applications, as is currently the case (Serjun et al., 2013), utilizing the raw material to produce high-performance by-product-based construction materials like LSG can have both environmental and economic benefits.

Fiber hybridization is a favorable option to overcome some of

* Corresponding author.
E-mail address: mirja.illikainen@oulu.fi (M. Illikainen).

https://doi.org/10.1016/j.jclepro.2018.11.241
0959-6526/© 2018 The Authors. Published by Elsevier Ltd. This is an open access article under the CC BY-NC-ND license (http://creativecommons.org/licenses/by-nc-nd/4.0/).

the mechanical weaknesses in cementitious composites. There are mainly two approaches to employ hybrid fibers, namely fibers different in sizes (i.e., micro and macro fibers) and fibers different in elastic modulus (i.e., low and high modulus fibers) (Banthia and Nandakumar, 2003). In the literature, hybrid fibers were successfully used to develop high-performance cementitious composites or PSH composites using OPC-based matrices (Kang et al., 2016; Pakravan et al., 2016; Plizzari, 2005). In addition, hybrid fiber reinforcement was adopted in AAM composites recently (Goncalves et al., 2018; Kheradmand et al., 2017). However, there have been no investigations into hybrid-fiber-reinforced ettringite-based composites. Despite the considerable interest in improving the mechanical properties of LSG for applications in the constructions industry, the effects of hybrid fibers on the reinforcement of LSG are not yet known.

Therefore, the present experimental investigation aims to develop a cost-effective by-product-based LSG composite reinforced with different fibers. Encouraged by the need to better understand the mechanical properties of hybrid-fiber-reinforced ettringite-based binder, the study employed two types of PP fibers—namely multifilament PP (PP_{MF}) and split-film PP (PP_{SF}) fiber, and polyvinyl alcohol (PVA) fiber as fibrous reinforcement. Two combinations of fibers were also considered—namely hybrid PP fiber (i.e., PP_{MF}/PP_{SF}, in which PP_{MF} and PP_{SF} were combined) and hybrid PP and PVA fiber (i.e., PVA/PP_{MF}, in which PP_{MF} and PVA fiber were combined). In total, twelve combinations of materials (see details in section 2) were experimentally investigated to measure and compare the mechanical performance for the following relevant properties: flexural strength, compressive strength, fracture toughness, and uniaxial tensile strength. Finally, a multi-criteria ranking method was used to select the best mixture of the 12 different materials considering mechanical performance, cost, CO_2 footprint, and embodied energy.

2. Materials: components and manufacturing

2.1. Components

The LS was supplied by SSAB Europe Oy (Finland); it was collected at the slag cooling pit, and was exposed to natural weathering. The chemical composition of the LS (Table 1) was analyzed by X-ray fluorescence (XRF) (PANalytical Omnian Axiosmax) at 4 kV. The free CaO was zero and was measured by the method described in the standard EN 450-1. Moreover, the as-received LS was milled by a ball mill (TPR-D-950-V–FU-EH by Germatec, Germany) to reach a d_{50} value of less than 10 μm, as suggested by Adesanya et al. (2016). The particle size distribution was then analyzed by a laser diffraction technique with a Beckman Coulter 13 320. Fig. 1 shows the particle size distribution of raw materials used in this investigation.

Commercial gypsum ($CaSO_4.2H_2O$, supplied by VWR Finland, product code 22451.360) was used as a calcium sulfate source in this study. Gypsum was used to take advantage of its availability in secondary resources and to reduce energy consumption (Nguyen et al., 2019), instead of the dehydrated form gypsum ($CaSO_4$). The particle size distribution of gypsum is shown in Fig. 1, and the chemical component (analyzed by XRF) is indicated in Table 1. The mechanism and reactions to form ettringite were detailed in Nguyen et al. (2019), in which ettringite is the main crystalline hydrated product. Fig. 2 shows the XRD analysis of LSG after 1 and 28 days of curing in a humidity chamber (with a relative humidity of 95%, and a temperature of 23 °C) in comparison to the LS.

Table 1
Chemical composition (wt %) of LS, FBC-FA, and gypsum measured by XRF.

Oxide	CaO	SiO_2	Al_2O_3	Fe_2O_3	MgO	SO_3	Others
LS	50.96	8.27	27.87	1.13	6.31	0.80	4.66
Gypsum	41.40	0.96	0.12	0.07	0.48	53.75	3.22
FBC-FA	12.0	30.8	15.1	26.7	2.5	3.5	8.1

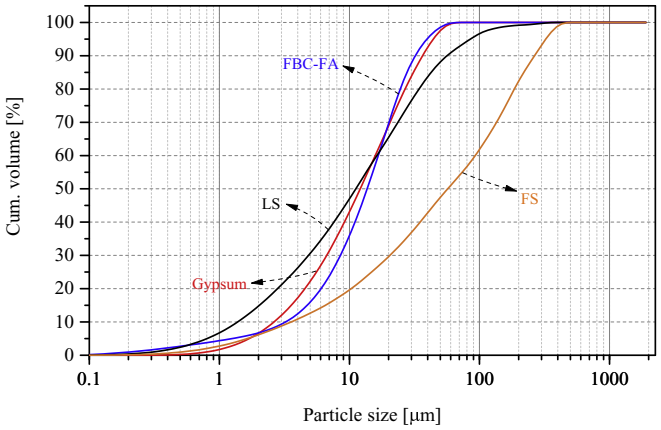

Fig. 1. Particle size distribution of raw materials, namely LS, FBC-FA. FS, and gypsum.

Citric acid (product code C1949 by Tokyo Chemical Industry Co., Ltd., Japan) was used as a retarder for the LSG in this investigation. Citric acid has been found to be an effective retarder in ettringite systems (Choi et al., 2016; Pelletier et al., 2010). The acid prevents nucleation and the subsequent crystal formation process of ettringite, as proposed by Cody et al. (2004). Based on the preliminary experiments in this investigation, 1.8% citric acid solution was used to attain the initial setting time of 1.2 h.

Fluidized bed combustion fly ash (FBC-FA) was employed as a filler in the LSG matrix, while fine sand (FS) was milled from standard sand according to EN 196-1. Particle size distribution of FBC-FA and FS are shown in Fig. 1. FBC-FA (provided by Oulun Energia, Finland) is also an industrial side stream from fluidized bed combustion with a relatively low CaO content (see Table 1) (as adopted by Rissanen Jouni et al., 2017). The fly ash was used to weaken the LSG matrix for better PSH behavior as well as to utilize the by-product from other industries along with slags from steel manufacturing. As suggested by Rissanen Jouni et al. (2017), 20% of FBC-FA was chosen to was chosen to reduce roughly 25% in compressive strength for the LSG matrix. As for the FS, Mustafa Sahmaran et al. (2009) reported that micro silica sand (particle size roughly 200 μm) is preferable for PSH cementitious composites, since the fine aggregate can help to achieve a uniform dispersion of fibers. In addition, the design framework for PSH composites based on micromechanical calculations (Li et al., 1995) suggested micro aggregates for better PSH behavior.

The hybrid fibers from the PP and PVA were used to enhance the mechanical properties of ettringite-based composites, including PSH behavior. The mechanical and physical properties of fibers are listed in Table 2. In an earlier study, the PP_{MF} and PP_{SF} fibers were successfully used in developing high-performance cementitious composite from LS (Nguyen et al., 2018). It is worth mentioning that using PP fiber is more cost efficient than other polymeric fibers (e.g., PVA and high-modulus polyethylene fibers). According to the design framework for PSH composites (Li et al., 1995; Nematollahi et al., 2016) and suggestions from Pakravan et al. (2016), the minimum fiber volume fraction of 2% was chosen to yield PSH behavior with hybrid-fiber-reinforced LSG composites with adequate workability. Table 3 details the fiber volume fraction and combinations of fibers used in the investigation.

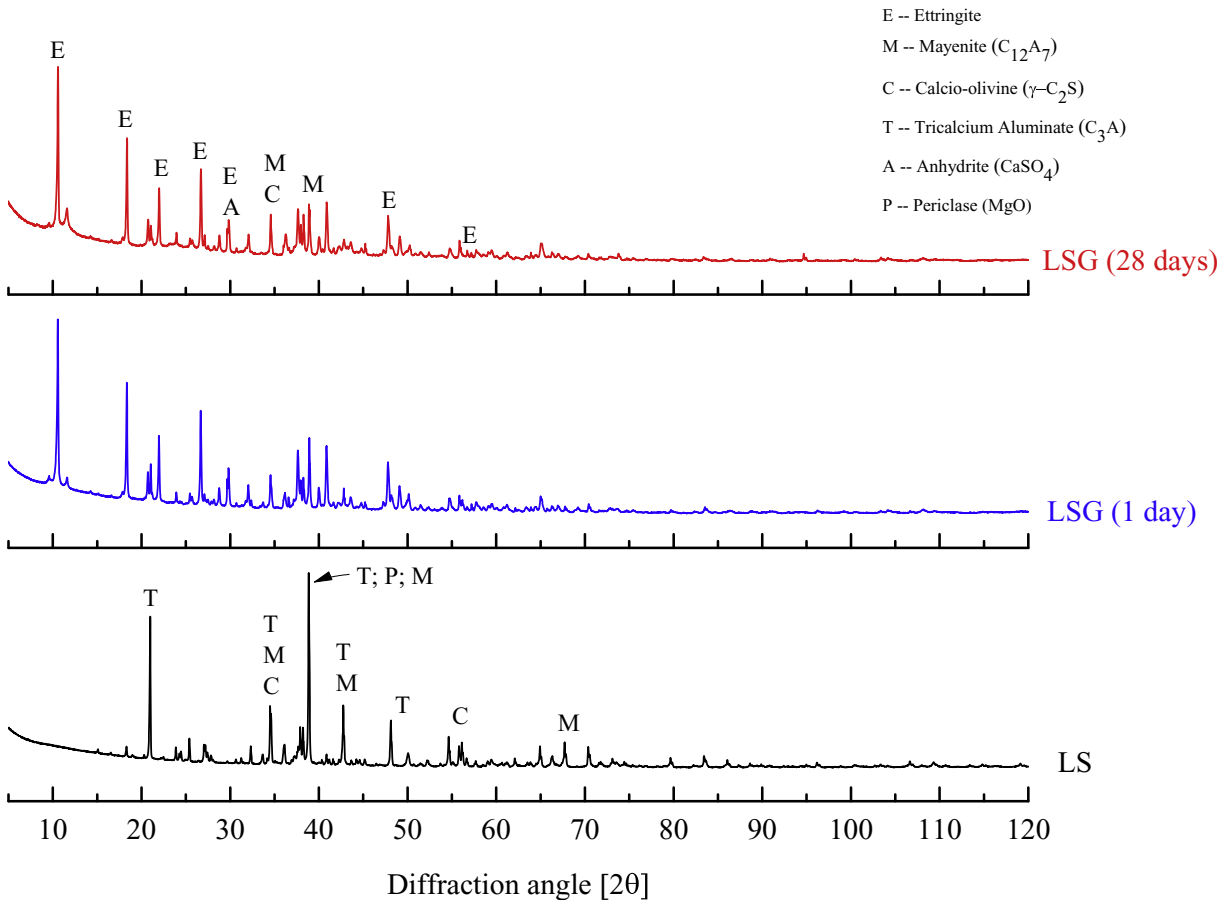

Fig. 2. XRD characterization of LSG at 1 and 28 days of age compared to as-received LS.

Table 2
Mechanical and physical properties of PP_{MF}, PP_{SF} and PVA fiber.

ID	Type	Young's modulus (GPa)	Elongation at break (%)	Tensile strength (MPa)	Length (mm)	Diameter (μm)	Density (g/cm^3)
PP_{MF}	Multi-fiber	9	22	910	10	12	0.91
PP_{SF}	Split-film fiber	4–6	12	340	20	38	0.91
PVA	Multi-fiber	41	6	1600	8	40	1.3

Table 3
Fiber volume fraction (vol. %) of investigated combinations on 2 matrices: LSG and LSG-FA.

Mix ID	PP_{MF}	PP_{SF}	PVA
Plain	–	–	–
PP_{MF}/PP_{SF}	1	1	–
PVA/PP_{MF}	1	–	1
PP_{MF}	2	–	–
PP_{SF}	–	2	–
PVA	–	–	2

2.2. Fiber-reinforced mortar preparation

The preparation of mortar specimens proceeded as follows: citric acid solution was prepared with a concentration of 1.8%, and the solution was then kept at room temperature (roughly 23 °C). LS, gypsum, FS, and FBC-FA (the latter only for LSG-FA matrix) were then weighted and mixed in a 5-L Kenwood mixer at a low and high speed (70 rpm and 150 rpm, respectively) for 1 min at each level. The citric acid solution was gradually added to the dry mixture. The mortar was mixed at a low speed for 3 min before the fibers were added into the mixture. The fibers were gradually added to the mortar to obtain uniform fiber distribution and to prevent fiber clustering during mixing. During the process, the mixing speed was kept at a low level, and the mortar was checked periodically to ensure uniform fiber dispersion in the mortar. After adding the fibers, mixing was continued for 10 min at a high speed. It took 20–25 min to complete the mixing process. Mortar samples were cast into molds, and vibrated for 3 min at a frequency of 1 Hz. The samples were cured in plastic bags at room temperature for 24 h before demolding. Then the samples were cured in a humidity chamber (with a relative humidity of 95%, and a temperature of 23 °C) for 7 days before testing. Due to the fast strength development of LSG (Nguyen et al., 2019), the mechanical properties at 7 days can represent the behavior of the materials at its final age. The volume fraction of the fibers and recipe of the two matrices (LSG and LSG-FA) are shown in Tables 3 and 4, respectively.

A superplasticizer and dispersing agent were employed to gain proper workability and fiber dispersion. The former was a melamine-based chemical specified for calcium sulfate cements, named Melment F10 and provided by BASF (Germany). The latter

Table 4
Mix weight proportions of the matrices LSG and LSG-FA.

Matrix ID	Slag	Gypsum	FBC-FA	W/B[a]	Citric acid[b]	Sand[c]
LSG	0.7	0.3	–	0.45	1.8%	0.5
LSG-FA	0.56	0.24	0.2	0.6		

[a] W/B (water-to-binder ratio) with total binder mass calculated by the sum of the mass of slag and gypsum.
[b] Citric acid mixed with water to produce solution with 1.8% concentration.
[c] Weight proportion of total mass of LS + gypsum (in LSG) or LS + gypsum + FBC-FA (in LSG-FA).

was a sodium polymethacrylate, named Darvan 7-N and supplied by Vanderbilt (USA). The dosage of the superplasticizer and dispersing agent were 0.5% and 1%, respectively, by the weight of the total binder mass.

3. Features of the mechanical tests

To assess the mechanical performance of the multi-fiber reinforced LSG, the following parameters were measured: flexural, compressive, and tensile strength, and fracture toughness. Uniaxial tension and flexural (notched and un-notched beams) tests were assisted by the 2D digital image correlation (DIC) technique to monitor the evolution of crack patterns. Images were captured and analyzed by LaVision StrainMaster (2016). The image acquisition frequency was set at 1 Hz, and the speckle pattern region of the sample was illuminated by a LED light source. The aperture and the shutter speed of camera were set to f/4.0 and 2000 μs, respectively. The post processing of images allowed the measurement of the full-field displacement and the calculation of the strain distribution over the surface, which was previously painted with white and speckled with black acrylic paints. Some of the adopted parameters for correlation were subset size 37 and step size 3. Those were selected because lower values of the subset and step sizes did not generate considerable variation of the calculated strain field.

After 7 days of curing, the 3-point bending for un-notched $4\times4\times16$-cm^3 prismatic specimens and compressive tests, according to the standard ISO 679-2009 (2009), were conducted by a Zwick device (load cell of 100 kN). At least 3 specimens for each material were tested to determine the flexural characteristics of the 12 mixtures. The 3-point bending test was displacement controlled with a speed rate of 0.4 mm/min. The compressive strength was measured by loading halves of the prismatic bending specimens. At least 4 specimens were tested for each material, setting a displacement speed of 1 mm/min.

The fracture toughness was investigated by the 3-point bending setup loading notched specimen, according to RILEM (1985). The 3-point bending test was conducted after 7 days by the same loading device for the bending tests. The displacement-loading rate was 0.4 mm/min. Fracture energy was calculated based on the recommendations of RILEM (1985), while the fracture toughness was computed by the effective crack model suggested by Karihaloo and Nallathambi (1990). More details of calculations and setup for the fracture toughness can be found in Nguyen et al. (2018).

Uniaxial tension tests were performed on dog-bone specimens, with the dimensions recommended by JSCE (2008). The adopted main geometrical features were the following: width of the grip zone at 60 mm, width of the free length at 30 mm, thickness at 13 mm, total length at 330 mm, and free length at 80 mm. The same specimen geometry was successfully used in previous investigations in the literature (e.g., Ohno and Li, 2014). The tensile tests were performed with a machine MTS 810 (maximum load capacity set to 10 kN), with a loading rate of 0.5 mm/min.

4. Results and discussion

The experimental results provide details about the mechanical properties of the developed cementitious composites through different characterizations and mechanical testing. The comparisons are based on three main aspects: the effect of the fibrous reinforcement, the differences between the two matrices, and the combination of fibers. Experimental results revealed that the developed composites attained excellent improvement in mechanical properties. Also, the effects of the fibers and of the matrices were distinguishable. However, the authors are aware of the influence of the random orientation of fibers, as well as the possible clustering, on the mechanical properties of the considered composites.

4.1. Bending

Fibers greatly enhanced the flexural strength of cementitious composites. Fig. 3a shows the flexural strength of all combinations under 3-point bending tests. The polyvinyl alcohol (PVA) fiber offered the most significant improvement in maximum load with roughly 140% and 220% greater than that of the plain compositions on LSG and LSG-FA, respectively. This effect was attributed to the hydrophilic nature of the fiber, as reported in other studies (e.g., Pakravan et al., 2016). On the other hand, PP fibers enhanced the bending strength of composites around 60–80% compared to the plain LSG and LSG-FA. Although the PP_{SF} fiber was coated with a hydrophilic layer, as reported in Nguyen et al. (2018), the interfacial bonding between the fibers and matrices was not as good as that of the PVA fiber. As for the matrices, the FBC-FA weakened LSG by approximately 40%. However, regardless the matrices, by using a proper amount of fibrous reinforcement, the flexural strength of composites generally increased by approximately 90% up to 220% (see PVA-LSG-FA).

Beside the flexural strength, the effects of fiber hybridization are clear in the post-peak behavior. Fig. 3b shows the average stress vs. mid-span deflection curves of 12 combinations divided into three blocks from left to right—namely reference materials, hybrid-fiber-reinforced compositions, and mono-fiber-reinforced compositions. The hybrid fiber combined the behavior with each mono fiber reinforcement, which can be clearly seen in PVA/PP_{MF}-LSG. The combination of PVA and PP_{MF} fibers offered a similar peak load with PVA-LSG, but larger energy was absorbed in the post-peak branch. The effect resulted from the combination of the hydrophilic nature of PVA fiber, which led to high bonding strength with the matrix and good energy absorbent with the PP_{MF} fiber (Felekoğlu et al., 2016). This behavior can also be seen on the other hybrid-fiber-reinforced mortars. For example, PP_{MF}/PP_{SF} had a similar flexural strength to PP_{SF} and PP_{MF} on both the LSG and LSG-FA matrix (see Fig. 3a); however, the post-peak branch complied with an average trend between the PP_{SF} and PP_{MF} fiber reinforced mortars. Moreover, it is worth mentioning that all the fiber reinforced cementitious composites exhibited deflection-hardening behavior under the 3-point bending tests with a peak load about two times higher than the initial-crack load.

The fluidized bed combustion fly ash (FBC-FA) weakened the LSG; hence, more cracks were generated, as observed by the DIC technique, along with distinguishable deflection-hardening behavior. Fig. 4 shows the crack patterns at the peak load of the 12 combinations. The plain materials (i.e., LSG and LSG-FA) exhibited brittle behavior with a single flat crack at the peak load and eventually suddenly-dropped load level (see Fig. 3b). In contrast, other reinforced materials generated multiple cracks; a steady-state crack development led to deflection-hardening behavior (Yang et al., 2008). Comparing the matrices with and

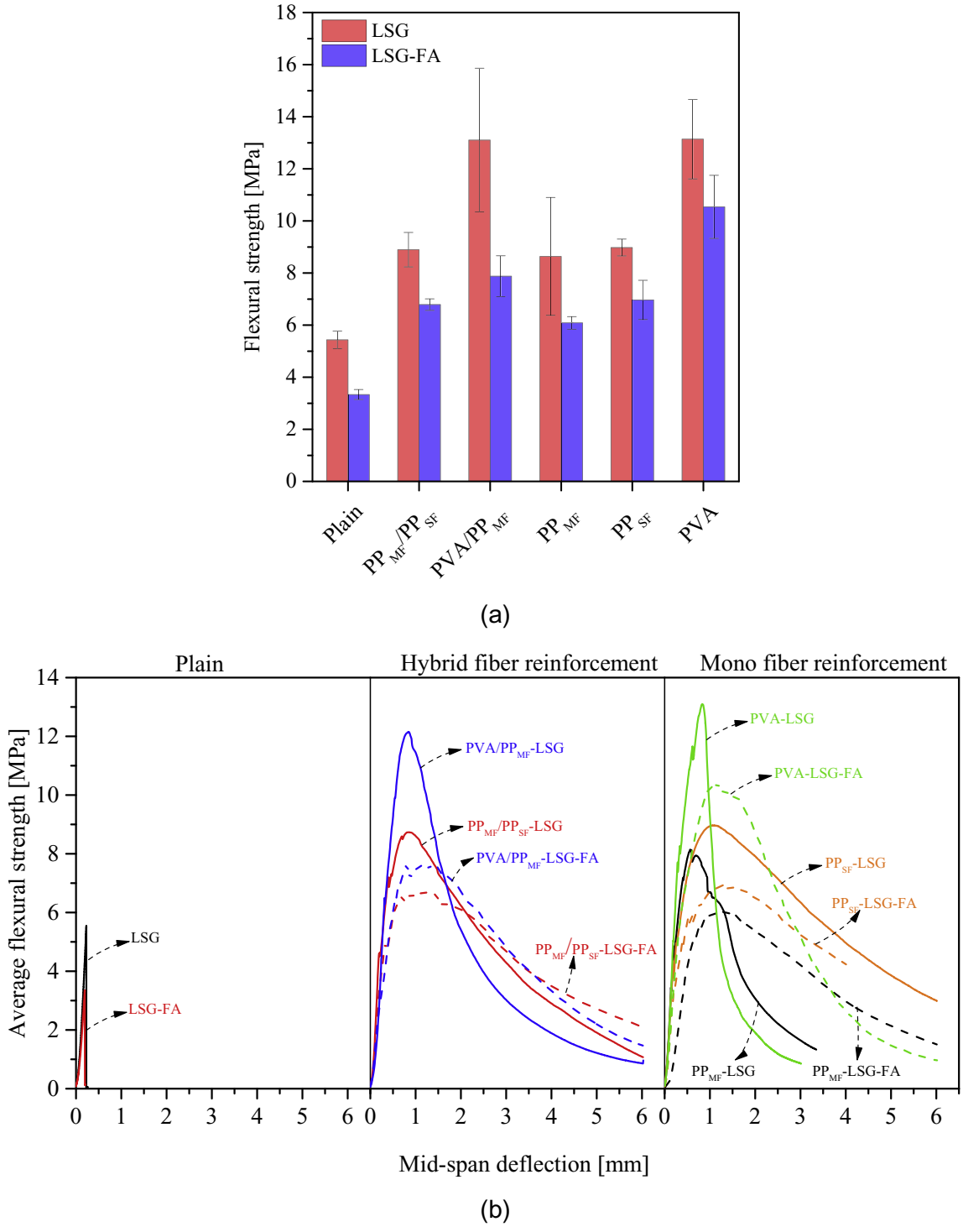

Fig. 3. Flexural tests: (a) flexural strength after 7 days curing (average and standard deviation of three tests); (b) average stress vs. mid-span deflection curves of 12 combinations; the averaged curves were computed by performing linear interpolation on data range input.

without FBC-FA, it can be clearly seen that LSG-FA generated more cracks, especially with the hybrid fibers (i.e., PP_{MF}/PP_{SF} and PVA/PP_{MF}) and the PVA fiber reinforced composites. It is due to the weaker matrix and the good interfacial bonding of PVA fiber and/or the bridging effect of fiber hybridization (i.e., PP_{MF}/PP_{SF}), which led to the load transferring from fibers to matrix and through the crack and consequently resulting in another crack in other flaw position of the matrix (Yang et al., 2008). This repeated process resulted in multiple crack formations (Fig. 4) and, as observed, deflection-hardening behavior (Fig. 3b).

The scanning electron microscopy (SEM) images on crack surfaces of LSG and PVA-LSG confirmed the bridging action and interfacial bonding properties of the fibers (Fig. 5). The fracture surface of unreinforced material showed typical brittle failure with crack propagation along the interfacial transition zone between matrix and FS (Fig. 5a). As reported in a previous work (Nguyen

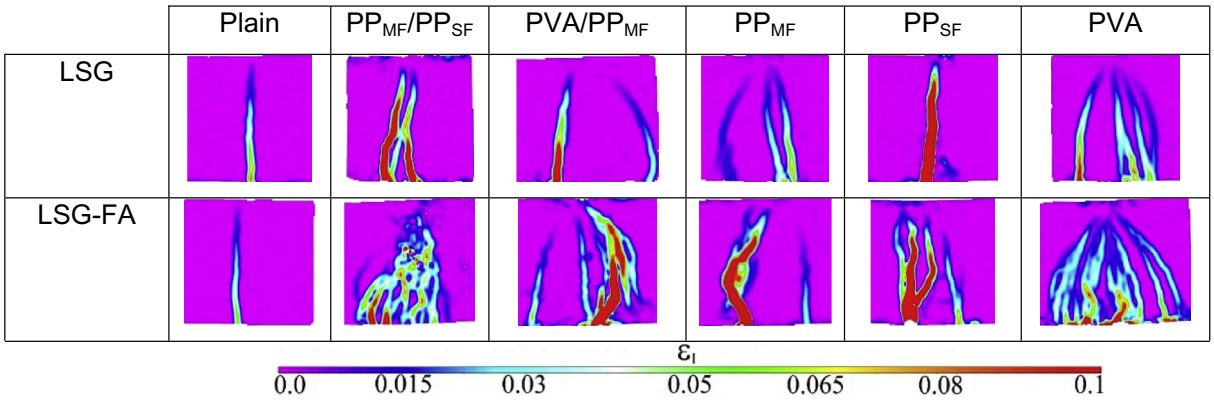

Fig. 4. Flexural tests: Contour of the maximum principal strain by the DIC technique at the maximum bending load of 12 combinations after 7 days of curing.

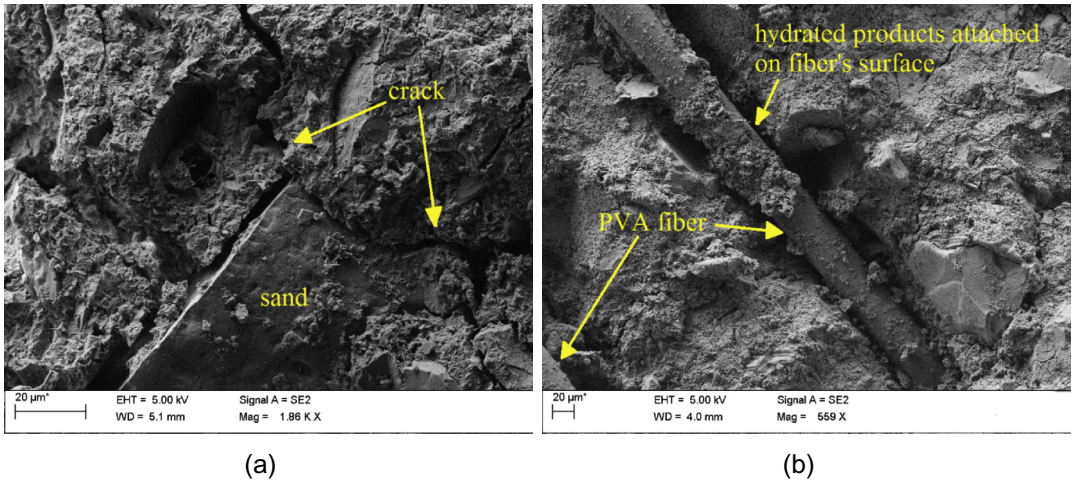

Fig. 5. Flexural tests: SEM images on fracture surfaces of (a) unreinforced material (LSG) and (b) fibers reinforced composites (PVA-LSG).

et al., 2019), the SEM images revealed that the main crystalline phase in LSG is ettringite, which is generated from the chemical reaction between LS and gypsum. The SEM image of the reinforced composite (i.e., PVA-LSG) showed that PVA fibers failed by debonding (Fig. 5b). Nedeljković et al. (2018) observed a combination of fiber pullout and rupture in the PVA fiber reinforced AAM. In addition, the fibers had some residual hydrated products attached on the surface, showing good bonding between fibers and matrix. This good bonding strength, hence, resulted in an efficient load carrying capacity and multiple cracks at the macro scale, as showed in Figs. 3 and 4. The fiber-reinforced composites absorbed a much larger amount of energy for propagating cracks, resulting in high ductility.

4.2. Unconfined compression

The fibrous reinforcement greatly improved the compressive strength of composites on LSG matrix, compared to the plain material. Fig. 6 shows the average results of compressive strength measured after 7 days of curing. Reinforced LSG mortars increased their strength up to 130% in comparison to the unreinforced materials. This improvement is due to the fiber bridging action on cracks, which restrained the crack propagation. Furthermore, the fibers reduced the extent of stress concentration at the crack tip; hence, they delayed the growth rate of cracks (Afroughsabet and Ozbakkaloglu, 2015; Yan et al., 1999). In addition, the hybridization of PP fibers offered a better increment in compressive strength than mono PP_{MF} and PP_{SF} fibers (roughly 15% higher). The micro and macro PP fibers played different roles in delaying the propagation of different crack sizes. On the other hand, the combination of PVA and PP_{MF} seems to have no advantages compared to the mono PVA fiber. However, it is worth noting that both PVA-LSG and PVA/PP_{MF}-LSG had the highest compressive strength (approximately 50 MPa) compared to all other compositions because of the good bonding strength between the hydrophilic PVA fibers and LSG.

In contrast, the fibers in LSG-FA matrix did not offer similar improvement to the compressive strength of the developed composites. The maximum increase was around 40%, featured by the mono PVA fiber. The PP_{MF}-LSG-FA reduced the compressive strength by approximately 6%, which could be considered in the experimental scatter band. The matrix with the fly ash might become more porous, which makes the initiation and the growth of cracks easier and faster (Sukontasukkul et al., 2018). Kang et al. (2016) reported a similar reduction with maximum 14.1% on the compressive strength of the hybrid-fiber-reinforced ultra-high performance concrete.

4.3. Fracture toughness

The fiber reinforced composites had excellent load carrying capacity due to the fiber bridging action, while the plain material

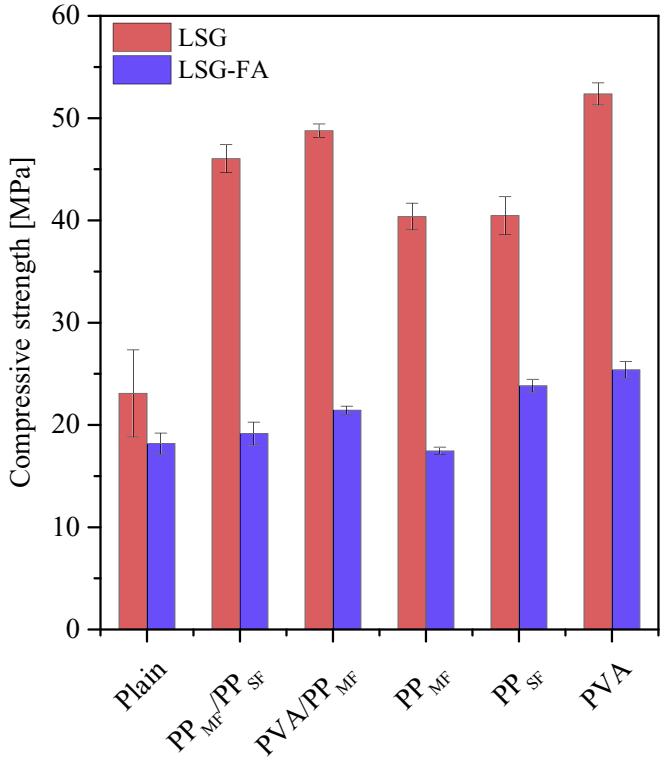

Fig. 6. Compressive strength of materials after 7 days of curing (average and standard deviation of 4 tests).

showed typical brittle failure under a mode I fracture. Fig. 7 shows the average load vs. crack mouth opening displacement (CMOD) curves of all 12 combinations. The CMOD was measured by the DIC technique. The fibers dramatically improved the peak load and post-peak branch. After the onset of the initial crack, the fibers started bridging and absorbing energy immediately. The only exception was PP_{SF}-LSG, which had a significant drop in the load level after the first crack appeared. This behavior could be attributed to the weakening effect of FBC-FA, as a filler, leading to an earlier diffusion of micro cracking in the LSG-FA matrix than in the LSG matrix. This is visible considering the early deviation from linearity of the load-CMOD curve of PP_{SF}-LSG-FA as compared to the PP_{SF}-LSG counterpart. Therefore, the dimensions of the PP_{SF} fibers allowed the bridging action in LSG-FA to start earlier that than in LSG, and it allowed a higher load carrying capacity of the material.

Furthermore, the CMOD at peak load measured by the DIC technique (Fig. 8) showed the distinguishable CMODs of reinforced and plain materials. At the peak load, the crack of the reinforced compositions on both LSG and LSG-FA matrix was open wide and exhibited a very high ductility. In contrast, the plain material had a very small crack opening and also a lower peak load than that of the reinforced materials. For instance, the CMOD attained roughly 1.3 mm at the peak load (i.e., 520 N) of PP_{SF}-LSG-FA, compared to a CMOD of around 0.01 mm for the plain LSG-FA at approximately 240 N. Furthermore, it is important to note that when the multiple cracks appeared at the notch tip during the 3-point bending tests (e.g., see PVA/PP_{MF}-LSG-FA in Fig. 8), the CMOD measured by the DIC technique could not provide a comprehensive representation of the material properties, as reported by Paegle et al. (2016). Therefore, in this study, only samples that had the start of a single crack from the notch were considered as representative results for the fracture toughness test.

Fracture energy was radically increased for all fiber reinforced composites, but the effect on fracture toughness was less considerable. Fig. 9 shows the two parameters for all combinations. For the PP_{MF} fiber, the fracture energy of the composites on both LSG and LSG-FA was almost the same (around 3.8 N/mm). However, the fracture toughness of the PP_{MF}-LSG was about 1.5 times higher than that of the PP_{MF}-LSG-FA. The better bonding strength between the fibers and matrices led to higher peak load under the mode I fracture (see Fig. 7) and, consequently, to higher fracture toughness. This agreed with the compressive strength of the two materials shown in Fig. 6. Similar performance was seen in the mono PVA fiber reinforced LSG and LSG-FA. A positive effect of the FBC-FA on fracture energy and toughness was on the composite reinforced with PP_{SF}, as discussed above. In contrast, the hybrid fibers (i.e., PP_{MF}/PP_{SF} and PVA/PP_{MF}) reinforced matrices exhibited opposite behavior, although the considerable scatter cannot lead to a general conclusion, and further in-depth analysis is needed. For instance,

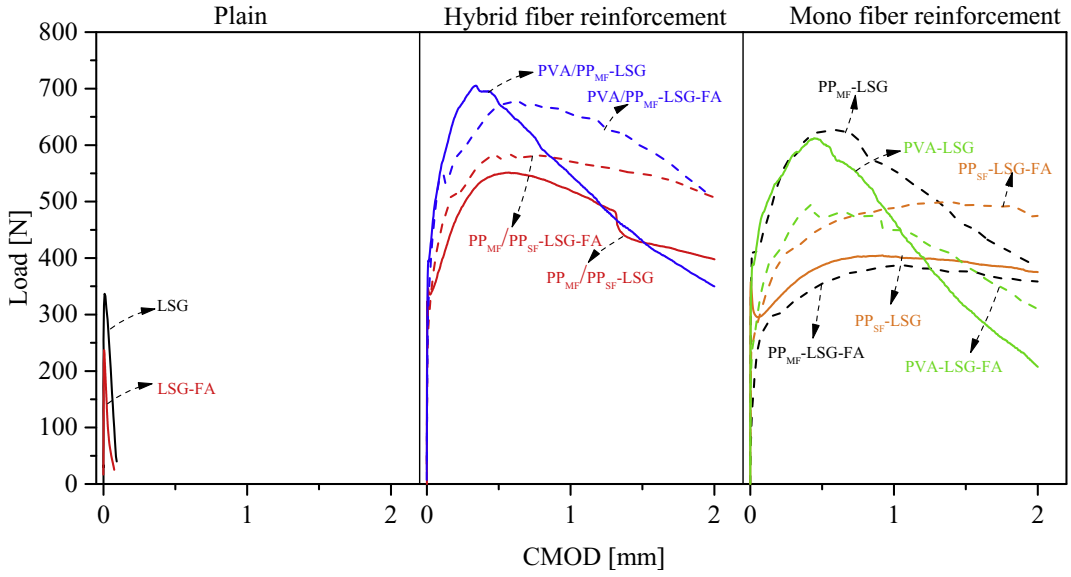

Fig. 7. Fracture toughness tests: average load vs. CMOD curves of 12 combinations.

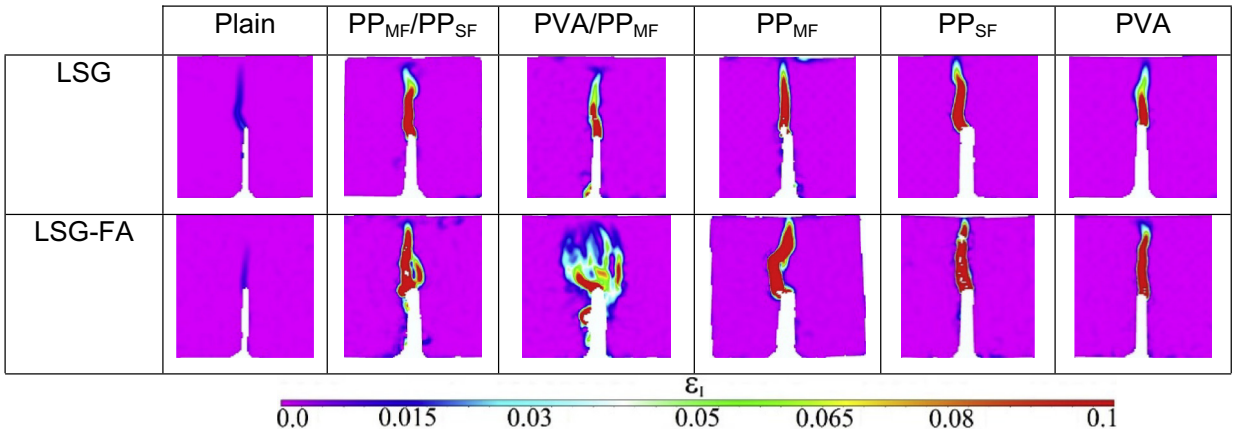

Fig. 8. Fracture toughness tests: contour map of the maximum principal strain captured by the DIC technique at the peak load of 12 combinations.

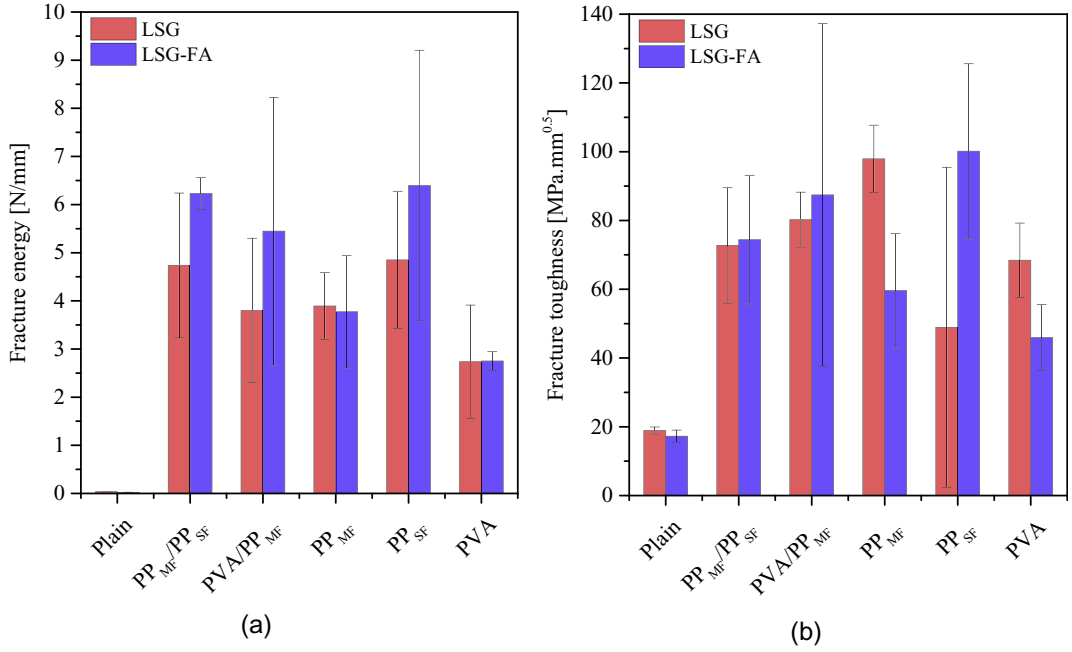

Fig. 9. Fracture toughness tests: (a) fracture energy and (b) fracture toughness at failure (average and standard deviation of 3 tests).

the fracture energy of the PP_{MF}/PP_{SF} on the LSG-FA was larger, but the fracture toughness was similar to that of hybrid PP fibers reinforced LSG. Furthermore, it can be seen from both parameters that the PP_{MF}/PP_{SF} fiber combined the effects of two mono fibers, and attained moderate values when compared to that of the PP_{MF} and PP_{SF} fiber reinforced composites regardless the matrix type.

In general, the fibers greatly enhanced fracture toughness and energy to mortars. Reinforced composites could attain a fracture energy and toughness at more than 160 and 5 times, respectively, higher than the plain materials. The results are comparable with those reported by Alomayri et al. (2014) and Nguyen et al. (2018). Moreover, the FBC-FA did not jeopardize the fracture energy, and it was increased by using the PP_{MF}/PP_{SF}, PVA/PP_{MF}, and PP_{SF} fibers, as compared to that of the LSG matrix. The relatively low fracture toughness of the PVA fiber reinforcement (see Fig. 9b) was related to the low ductility of the fibers. On the other hand, the PP_{MF} fiber reinforcement contributed more to ductile behavior due to slower reduction of load carrying capacity because of fiber pull-out (Felekoğlu et al., 2016). Therefore, the fiber hybridization of the PVA and PP_{MF} fibers is favorable to enhance the absorbed energy.

4.4. Uniaxial tension

The PSH behavior was recorded on fibers reinforced composites under uniaxial tension tests. Fig. 10a shows the comparison between the average stress vs. strain (measured by the DIC technique) curves of the 12 combinations. The plain materials exhibited a typical stress-strain curve for brittle materials, in which the stress dropped immediately after reaching the peak load with a very small strain. In contrast, other reinforced mortars attained PSH behavior after the onset of an initial crack with different strain capacity and peak load from one another. The strain capacity (i.e., strain at max stress) of reinforced mortars ranged from 0.5 to 1.3% for almost all combinations. Exceptionally, the PP_{SF}-LSG prolonged the load level as high as the initial crack load up to a 2.5% strain. On the other hand, PVA and PVA/PP_{MF} fiber on LSG matrix obtained a poor strain

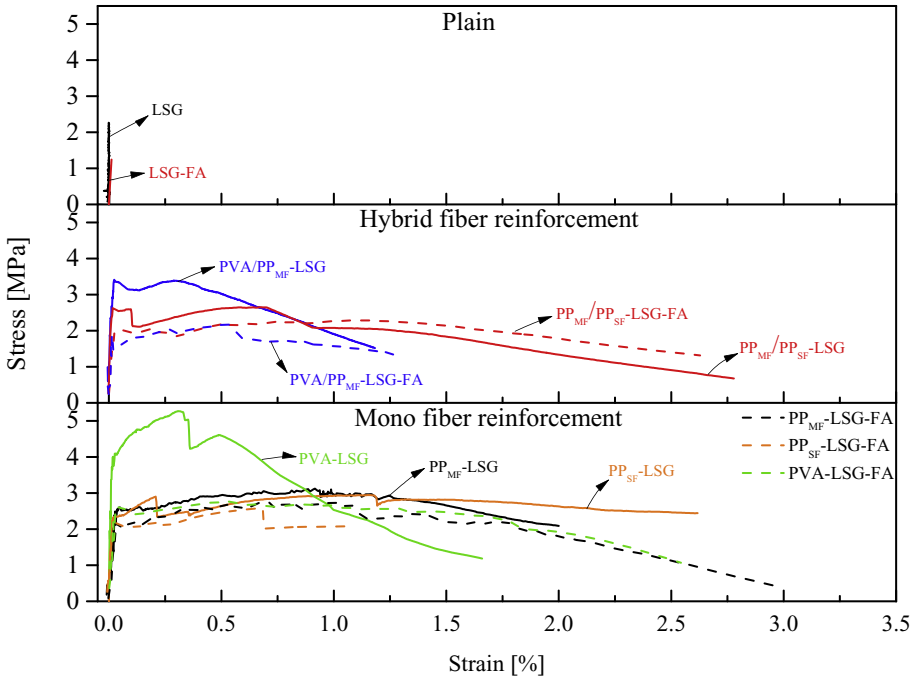

(a)

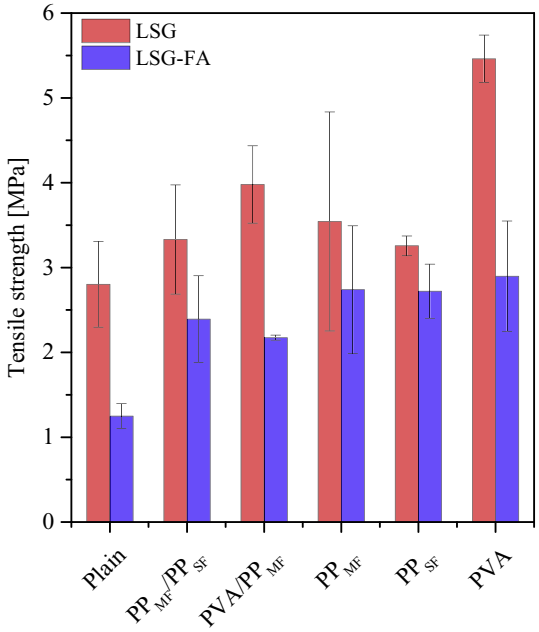

(b)

Fig. 10. Tensile tests: a) average stress vs. strain curves b) tensile strength of the 12 combinations (average and standard deviation of 3 tests).

capacity due to PVA lower ductility under tension. However, after the initial crack onset, the developed composites showed PSH behavior due to a proper load transferring mechanism with an increase in the peak load of up to approximately 45% in comparison to the initial crack load (i.e., PVA-LSG). Similar results in the literature were reported on the OPC cement-based ECC using hybrid PP-PVA fibers (Pakravan et al., 2016).

The PVA fiber enhanced the tensile strength of the developed composites significantly on both the LSG and LSG-FA matrix. Fig. 10b shows the tensile strength of all developed composites under uniaxial tension. The reinforced composites increased the tensile strength by roughly 100% in comparison to the plain LSG-FA. Interestingly, the hybrid fibers seemed to have no advantages compared to the mono fibers. As for the LSG matrix, the effects of the PP and its hybrid fiber were distinguishable from that of the PVA and PVA/PP$_{MF}$ fiber. Compared to the plain LSG, the PP fibers enhanced the tensile strength by roughly 25%. In addition, there was no clear effect of the PP fiber combination on the tensile strength; this behavior was also indicated in the stress vs. strain curves in Fig. 10a. In contrast, the PVA fiber offered a better

improvement on the tensile strength than its hybrid combination (i.e., PVA/PP_{MF}). The tensile strength of PVA-LSG was 110% higher than the plain LSG, while that of the PVA/PP_{MF}-LSG attained an increase of around 30%. As noted by Felekoglu et al. (2014), curing conditions might affect the tensile properties and performance of the PP fiber reinforced composites. Therefore, further investigation into the effects of curing conditions on fiber reinforced LSG and LSG-FA matrices is recommended.

5. A multi-criteria ranking method

To optimize the mixture compositions regarding mechanical performance, cost, embodied energy, and CO_2 footprint, a multi-criteria ranking method was used. The ranking results indicated that PP fiber reinforced LSG composites obtained the best ranking, while other mixtures were sensitive to the dependent variables. However, depending on the applications of materials, the ranking could change to adapt to different purposes.

5.1. Features of the ranking method

The ingredients in the mixtures were the independent variables; the dependent variables (i.e.., mechanical properties, cost, embodied energy, and CO_2 emission) changed based on the independent variables (Mastali et al., 2018). In this investigation, the method based on Equations (1)–(3) was used to rank the mixture compositions based on mechanical performance, cost, embodied energy, and global warming intensity (GWI). The ranking suggested the most suitable mixture among the given alternatives. This technique was also adopted for other studies on recycled steel fiber reinforced concrete for optimization purposes (Mastali et al., 2018; Sengul, 2016).

$$d_j = \left[\frac{Y_j - minf_j}{maxf_j - minf_j}\right]^{t_j} \quad (1)$$

$$d_j = \left[\frac{maxf_j - Y_j}{maxf_j - minf_j}\right]^{t_j} \quad (2)$$

$$D = (d_1 \times d_2 \times d_3 \times \ldots \times d_m)^{\frac{1}{m}} \quad (3)$$

Where: Y_j is the result of the *j-th* parameter for a considered mixture; $minf_j$ and $maxf_j$ are the lowest and the highest results, respectively, of the *j-th* parameter over all the mixtures included in the ranking; t_j is a weighting factor of the *j-th* parameter; all weighting actors t_j are set to 1, so no parameter is more important than another; and m is the number of parameters.

In this study, eight parameters were considered in the ranking. The mechanical properties consisted of flexural, compressive, and tensile strength, fracture energy, fracture toughness, and tensile strain capacity as detailed in Section 4. As for the costs and embodied energy of the mixtures, these parameters were only depended on the mass fraction of the different fibers because LS and FBC-FA were industrial by-products and, hence, were considered to have no significant difference in embodied energy. According to (Kua, 2015) and (Ohno and Li, 2018), the embodied energy of slag and fly ash was roughly 0.59 and 0.11 MJ/kg, respectively. Therefore, the results were calculated with the mass fraction of each fiber type and the costs or energy per kilogram of the fibers. The costs of PVA and PP fiber were approximately 12.2 €/kg and 0.8 €/kg (Pakravan et al., 2017), respectively. The embodied energy of the former and the latter was 107 MJ/kg (Nematollahi et al., 2017) and 84 MJ/kg (Bartl, 2009), respectively.

Table 5
GWI of raw ingredients and curing using in concrete, ECC, EGC. LSG, and LSG-FA.

Ingredient[a]	GWI (kg CO_2-eq/kg)
Portland cement	0.93
Coarse/Fine aggregate	0.0062
FS	0.025
Fly ash	0.0074
PVA or PP fiber	3.4
Super plasticizer	1.5
Water	0
NaOH	0.86
Na_2SiO_3	0.43
LS	0.0127
Gypsum[b]	0.051
Curing[c]	40

[a] Data adopted from Kua (2015); Ohno and Li (2018); and Yin (2017).
[b] Data adopted from Fořt and Černý (2018) for processing natural gypsum from quarrying raw material to storing crushed gypsum.
[c] Turner and Collins (2013) assumed that liquid petroleum gas, used in the curing process, was estimated about 40 kgCO_2-eq for 1 m^3 geopolymer.

These values show that the fraction of PVA fiber must be minimized to get an economical mixture. Ohno and Li (2018) suggested the similar scheme for optimizing the PVA fiber used in engineered geopolymer composites (EGC).

Regarding the GWI, the CO_2 footprint of fiber reinforced LSG and LSG-FA composites was almost the same with each other and was much lower than the other conventional concrete and engineered cementitious composites (ECC). The GWI of raw ingredients are shown in Table 5. Fig. 11 compares the GWI of the LSG and LSG-FA composites to that of an air-entrained (AE) concrete, a typical ordinary Portland cement (OPC)-based ECC (i.e., ECC M45), a high-volume fly ash (HVFA) ECC, and an EGC with 2% v/v fiber fraction (i.e., ECC-2%), as reported by Ohno and Li (2018). The by-product-based composites, developed in this study, produced approximately 147 kg CO_2-eq/m^3—roughly 4 times lower emission than the ECC M45. Moreover, the ettringite-based composites released

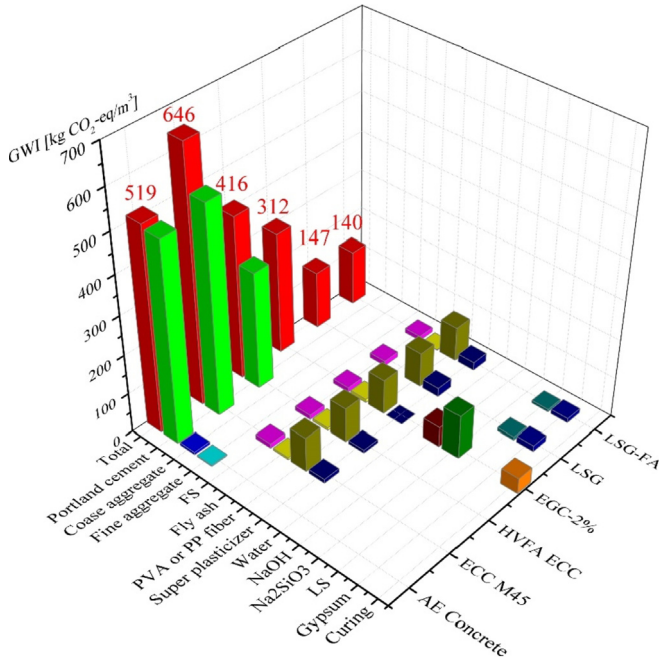

Fig. 11. GWI for fiber reinforced the LSG and LSG-FA in comparison to AE concrete, ECC M45, HVFA-ECC, and EGC with 2% v/v fiber fraction (adopted from Ohno and Li, 2018).

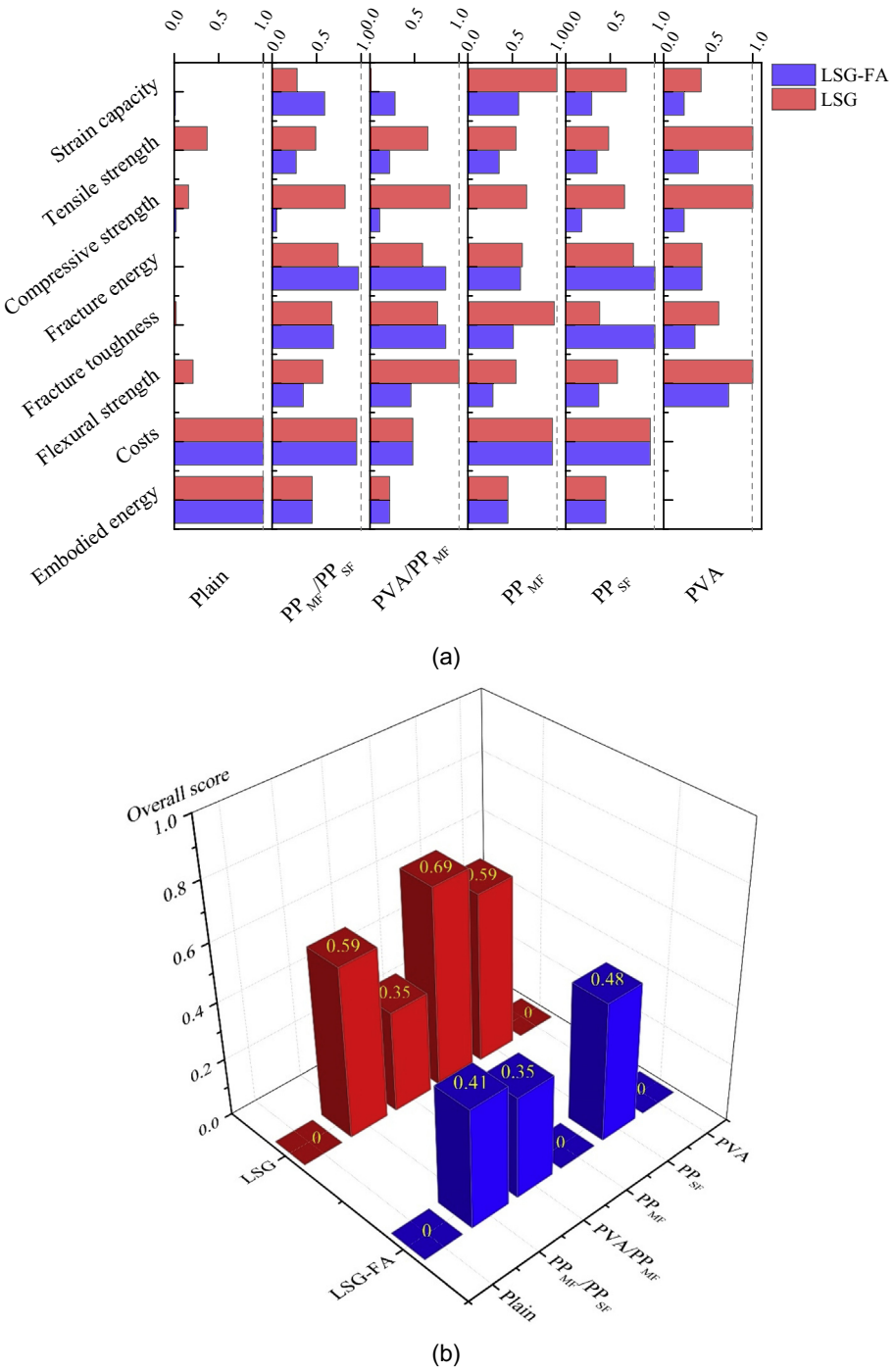

Fig. 12. (a) Individual and (b) overall desirable functions of the mixtures based on the multi-criteria ranking method.

almost 60% less CO_2 gas than the EGC, which used alkali activators (i.e., NaOH and Na_2SiO_3) (Ohno and Li, 2018). In addition, the EGC, LSG and LSG-FA were promising alternatives to other OPC-based concretes, namely the AE concrete, ECC M45, and HVFA ECC. It can be seen that the OPC occupied the main proportion in the CO_2 footprint of the conventional concretes (e.g., up to 98% in the AE concrete). Therefore, by using industrial wastes or by-products as cementitious materials, the greenhouse gas emission reduced significantly. It is worth mentioning that using waste gypsum can reduce even more the CO_2 emission of the developed composites. Furthermore, the PP and PVA fibers had almost the same CO_2 footprint (approximately 3.4 kg CO_2-eq/kg) (Ohno and Li, 2018; Yin et al., 2016). Therefore, the gas emission of all 12 combinations, investigated in this study was identical.

5.2. Ranking and comparison

The PP and PP_{MF}/PP_{SF} fiber reinforced LSG composites are the top 3 most favorable materials (i.e., PP_{MF}-LSG, PP_{SF}-LSG, and PP_{MF}/PP_{SF}-LSG), according to the assumptions in this study. Fig. 12 shows the individual and overall desirable functions of the mixture compositions, according to the multi-criteria ranking method of

both the LSG and LSG-FA matrix. Among the 12 combinations, the PP_{MF}-LSG maximized mechanical performance and minimized costs and embodied energy within the input data of this study. On the other hand, the mono PVA fiber reinforced composites had an overall function of zero due to the high cost and embodied energy, although the materials had a very good mechanical performance. In addition, the plain materials were the best in cost and embodied energy because they did not contain fibers; however, the mechanical performance was much worse than the reinforced mortars. Importantly, because of the adopted formulation (see Equation (3)), the overall function was very sensitive, and one single value could have a considerable impact on the final score. For example, PP_{MF}-LSG-FA attained a much better mechanical performance than the plain LSG-FA, but it had the poorest compressive strength, which caused a zero in the overall score.

Depending on the application of the material, some less important parameters can be left out or the more important parameters can increase its weight in the ranking. If the mechanical performance is the most important parameter, then other factors (e.g., costs and embodied energy) can be neglected, and the ranking would then recommend the PVA-LSG as the best mixture composition. In addition, if the ability of PSH behavior and load carrying capacity after peak load is required than the other parameters, strain capacity should be weighted by a factor higher than 1. As a consequence, the PP_{MF}/PP_{SF}-LSG-FA or PP_{SF}-LSG-FA was more favorable due to a weaker matrix, which caused more cracks and a more pronounced PSH behavior as discussed in Section 4.

6. Conclusions

This study investigated the effects of the polypropylene (PP) and polyvinyl alcohol (PVA) fibers and their hybrid fibers on the mechanical properties of an ettringite-based binder. The fibers enhanced the mechanical performance of the binder significantly under different loading conditions, namely flexural, compressive, and uniaxial tensile loading. Hardening behavior was observed on the developed composites with multiple cracks and prolonged post-peak branch.

The hybrid-fiber-reinforced mortar had comparable mechanical properties to the mono-fiber-reinforced mortar. Since the mixture of the two fibers could combine the mechanical properties of both fibers, the mechanical performance of hybrid-fiber-reinforced ettringite-based composites were mostly between those of mono-fiber-reinforced mortars.

The fluidized bed combustion fly ash (FBC-FA) was added to better utilize different by-products and to weaken the ettringite-based matrix (i.e., LSG), achieving better PSH behavior. As a counterpart, the compressive strength of the LSG-FA reduced by up to 60% compared to the LSG. To minimize the strength reduction while maximizing the enhancement in post peak behavior, the optimal FBC-FA dosage must be studied in further investigations.

The multiple criteria ranking method suggested the best mixture to attain the balance between mechanical performance, costs, and environmental impacts of the fiber reinforced composites. The PP_{MF} fiber reinforced LSG with 2% fiber volume fraction obtained the highest ranking, meaning the composite had the best balance between mechanical properties, costs, and embodied energy when all are appreciated evenly. However, depending on the requirements for the structural applications of the material, the ranking parameters could be adjusted to suit different purposes. In addition, there was no such difference in terms of CO_2 footprint between the two matrices developed in this study (i.e., the LSG and LSG-FA); both matrices offers much lower CO_2 emission than the other ordinary Portland cement (OPC)-based composites and the EGC.

Finally, this provides a better understanding of how mechanical behavior and environmental impact of industrial by-products can produce high-performance fiber reinforced cementitious composites with high utilization potential. Further investigations are needed in order to study the damage mechanisms at the micro-scale, the role of hydration products in the mechanical properties of LSG and LSG-FA, and the durability of the reinforced cementitious composites in aggressive environments.

Acknowledgements

This work was supported by the European Regional Development Fund [grant number: A70189]. The authors appreciate support from Brasilit Saint-Gobain (Brazil), Baumhueter Extrusion GmbH (Germany), Kuraray (Japan), SSAB Europe Oy (Finland), BASF (Germany), and Vanderbilt (USA) for providing the PPMF, PPSF, PVA fibers, the LS, the superplasticizer, and the dispersing agent, respectively. Hoang Nguyen gratefully acknowledges the financial support from the Tauno Tönning Foundation and valuable discussions with Mohammad Mastali (Ph.D., University of Oulu).

References

Adesanya, E., Ohenoja, K., Kinnunen, P., Illikainen, M., 2016. Alkali activation of ladle slag from steel-making process. J. Sustain. Metall. 1–11. https://doi.org/10.1007/s40831-016-0089-x.

Adesanya, E., Ohenoja, K., Kinnunen, P., Illikainen, M., 2017. Properties and durability of alkali-activated ladle slag. Mater. Struct. 50, 255. https://doi.org/10.1617/s11527-017-1125-4

Afroughsabet, V., Ozbakkaloglu, T., 2015. Mechanical and durability properties of high-strength concrete containing steel and polypropylene fibers. Construct. Build. Mater. 94, 73–82. https://doi.org/10.1016/j.conbuildmat.2015.06.051

Alomayri, T., Shaikh, F.U.A., Low, I.M., 2014. Synthesis and mechanical properties of cotton fabric reinforced geopolymer composites. Compos. B Eng. 60, 36–42. https://doi.org/10.1016/j.compositesb.2013.12.036

Banthia, N., Nandakumar, N., 2003. Crack growth resistance of hybrid fiber reinforced cement composites. Cement Concr. Compos. 25, 3–9. https://doi.org/10.1016/S0958-9465(01)00043-9

Bartl, A., 2009. Fiber Recycling: Potential for Saving Energy and Resources. International Solis Waste Association, Wien, Austria.

Choi, S., Kim, J.-M., Han, D., Kim, J.-H., 2016. Hydration properties of ladle furnace slag powder rapidly cooled by air. Construct. Build. Mater. 113, 682–690. https://doi.org/10.1016/j.conbuildmat.2016.03.089

Cody, A.M., Lee, H., Cody, R.D., Spry, P.G., 2004. The effects of chemical environment on the nucleation, growth, and stability of ettringite [Ca3Al(OH)6]2(SO4)3·26H2O. Cement Concr. Res. 34, 869–881. https://doi.org/10.1016/j.cemconres.2003.10.023

Duxson, P., Provis, J.L., Lukey, G.C., van Deventer, J.S.J., 2007. The role of inorganic polymer technology in the development of 'green concrete.' Cement Concr. Res. 37, 1590–1597. https://doi.org/10.1016/j.cemconres.2007.08.018

Felekoglu, B., Tosun-Felekoglu, K., Ranade, R., Zhang, Q., Li, V.C., 2014. Influence of matrix flowability, fiber mixing procedure, and curing conditions on the mechanical performance of HTPP-ECC. Compos. B Eng. 60, 359–370. https://doi.org/10.1016/j.compositesb.2013.12.076

Felekoğlu, B., Tosun-Felekoğlu, K., Keskinateş, M., Gödek, E., 2016. A comparative study on the compatibility of PVA and HTPP fibers with various cementitious matrices under flexural loads. Construct. Build. Mater. 121, 423–428. https://doi.org/10.1016/j.conbuildmat.2016.06.004

Fořt, J., Černý, R., 2018. Carbon footprint analysis of calcined gypsum production in the Czech Republic. J. Clean. Prod. 177, 795–802. https://doi.org/10.1016/j.jclepro.2018.01.002

Goncalves, J.R.A., Boluk, Y., Bindiganavile, V., 2018. Crack growth resistance in fibre reinforced alkali-activated fly ash concrete exposed to extreme temperatures. Mater. Struct. Constr. 51. https://doi.org/10.1617/s11527-018-1163-6

ISO 679, 2009. Cement – Test Methods – Determination of Strength, 2009. International Organization for Standardization.

Rissanen Jouni, Ohenoja Katja, Kinnunen Paivo, Illikainen Mirja, 2017. Partial replacement of portland-composite cement by fluidized bed combustion fly ash. J. Mater. Civ. Eng. 29, 04017061. https://doi.org/10.1061/(ASCE)MT.1943-5533.0001899

JSCE, 2008. Recommendations for design and construction of high performance fiber reinforced cement composites with multiple fine cracks. In: Concrete Engineering Series 82, Concrete Engineering Series. JSCE, Japan.

Juenger, M.C.G., Winnefeld, F., Provis, J.L., Ideker, J.H., 2011. Advances in alternative cementitious binders. Conf. Spec. Cem. Hydration Kinet. Model. Quebec City 2009 CONMOD10 Lausanne 2010 41, 1232–1243. https://doi.org/10.1016/j.cemconres.2010.11.012

Kang, S.-T., Choi, J.-I., Koh, K.-T., Lee, K.S., Lee, B.Y., 2016. Hybrid effects of steel fiber

and microfiber on the tensile behavior of ultra-high performance concrete. Compos. Struct. 145, 37–42. https://doi.org/10.1016/j.compstruct.2016.02.075
Karihaloo, B.L., Nallathambi, P., 1990. Effective crack model for the determination of fracture toughness (KIce) of concrete. Eng. Fract. Mech. 35, 637–645. https://doi.org/10.1016/0013-7944(90)90146-8
Kheradmand, M., Mastali, M., Abdollahnejad, Z., Pacheco-Torgal, F., 2017. Experimental and numerical investigations on the flexural performance of geopolymers reinforced with short hybrid polymeric fibres. Compos. B Eng. 126, 108–118. https://doi.org/10.1016/j.compositesb.2017.06.001
Kua, H.W., 2015. Integrated policies to promote sustainable use of steel slag for construction—a consequential life cycle embodied energy and greenhouse gas emission perspective. Energy Build.. 101, 133–143. https://doi.org/10.1016/j.enbuild.2015.04.036
LaVision StrainMaster [WWW Document], 2016. http://www.lavision.de/en/products/strainmaster/index.php. (Accessed 27 January 2017).
Li, V.C., Mishra, D.K., Wu, H.-C., 1995. Matrix design for pseudo-strain-hardening fibre reinforced cementitious composites. Mater. Struct. 28, 586–595. https://doi.org/10.1007/BF02473191
Luukkonen, T., Abdollahnejad, Z., Yliniemi, J., Kinnunen, P., Illikainen, M., 2018. One-part alkali-activated materials: a review. Cement Concr. Res. 103, 21–34. https://doi.org/10.1016/j.cemconres.2017.10.001
Mastali, M., Dalvand, A., Sattarifard, A.R., Illikainen, M., 2018. Development of eco-efficient and cost-effective reinforced self-consolidation concretes with hybrid industrial/recycled steel fibers. Construct. Build. Mater. 166, 214–226. https://doi.org/10.1016/j.conbuildmat.2018.01.147
McLellan, B.C., Williams, R.P., Lay, J., van Riessen, A., Corder, G.D., 2011. Costs and carbon emissions for geopolymer pastes in comparison to ordinary portland cement. J. Clean. Prod. 19, 1080–1090. https://doi.org/10.1016/j.jclepro.2011.02.010
Mustafa Sahmaran, M.L., Khandaker M.A. Hossain, Ravi Ranade, and Victor C. Li, Lachemi, M., Khandaker M. A., H., Ranade, R., Victor C, L., 2009. Influence of aggregate type and size on ductility and mechanical properties of engineered cementitious composites. Materials J. 106. https://doi.org/10.14359/56556
Nedeljković, M., Luković, M., van Breugel, K., Hordijk, D., Ye, G., 2018. Development and application of an environmentally friendly ductile alkali-activated composite. J. Clean. Prod. 180, 524–538. https://doi.org/10.1016/j.jclepro.2018.01.162
Nematollahi, B., Sanjayan, J., Shaikh, F.U.A., 2016. Matrix design of strain hardening fiber reinforced engineered geopolymer composite. Compos. B Eng. 89, 253–265. https://doi.org/10.1016/j.compositesb.2015.11.039
Nematollahi, B., Ranade, R., Sanjayan, J., Ramakrishnan, S., 2017. Thermal and mechanical properties of sustainable lightweight strain hardening geopolymer composites. Arch. Civ. Mech. Eng. 17, 55–64. https://doi.org/10.1016/j.acme.2016.08.002
Nguyen, H., Carvelli, V., Adesanya, E., Kinnunen, P., Illikainen, M., 2018. High performance cementitious composite from alkali-activated ladle slag reinforced with polypropylene fibers. Cement Concr. Compos. 90, 150–160. https://doi.org/10.1016/j.cemconcomp.2018.03.024
Nguyen, H., Kinnunen, P., Carvelli, V., Mastali, M., Illikainen, M., 2019. Strain hardening polypropylene fiber reinforced composite from hydrated ladle slag and gypsum. Compos. B Eng. 158, 328–338. https://doi.org/10.1016/j.compositesb.2018.09.056
Ohno, M., Li, V.C., 2014. A feasibility study of strain hardening fiber reinforced fly ash-based geopolymer composites. Construct. Build. Mater. 57, 163–168. https://doi.org/10.1016/j.conbuildmat.2014.02.005
Ohno, M., Li, V.C., 2018. An integrated design method of Engineered Geopolymer Composite. Cement Concr. Compos. 88, 73–85. https://doi.org/10.1016/j.cemconcomp.2018.02.001
Paegle, I., Minelli, F., Fischer, G., 2016. Cracking and load-deformation behavior of fiber reinforced concrete: influence of testing method. Cement Concr. Compos. 73, 147–163. https://doi.org/10.1016/j.cemconcomp.2016.06.012
Pakravan, H.R., Jamshidi, M., Latifi, M., 2016. Study on fiber hybridization effect of engineered cementitious composites with low- and high-modulus polymeric fibers. Construct. Build. Mater. 112, 739–746. https://doi.org/10.1016/j.conbuildmat.2016.02.112
Pakravan, H.R., Latifi, M., Jamshidi, M., 2017. Hybrid short fiber reinforcement system in concrete: a review. Construct. Build. Mater. 142, 280–294. https://doi.org/10.1016/j.conbuildmat.2017.03.059
Passuello, A., Rodríguez, E.D., Hirt, E., Longhi, M., Bernal, S.A., Provis, J.L., Kirchheim, A.P., 2017. Evaluation of the potential improvement in the environmental footprint of geopolymers using waste-derived activators. J. Clean. Prod. 166, 680–689. https://doi.org/10.1016/j.jclepro.2017.08.007
Pelletier, L., Winnefeld, F., Lothenbach, B., 2010. The ternary system Portland cement–calcium sulphoaluminate clinker–anhydrite: hydration mechanism and mortar properties. Cement Concr. Compos. 32, 497–507. https://doi.org/10.1016/j.cemconcomp.2010.03.010
Plizzari, G.A. L.G.S. A.M , 2005. Bending and uniaxial tensile tests on concrete reinforced with hybrid steel fibers. J. Mater. Civ. Eng. 17, 519–527. https://doi.org/10.1061/ (ASCE)0899-1561(2005)17:5(519)
Provis, J.L., 2017. Alkali-activated materials. Cement Concr. Res. https://doi.org/10.1016/j.cemconres.2017.02.009.
RILEM, 1985. Determination of the fracture energy of mortar and concrete by means of three-point bend tests on notched beams. Mater. Struct. 18, 287–290. https://doi.org/10.1007/BF02472918
Sengul, O., 2016. Mechanical behavior of concretes containing waste steel fibers recovered from scrap tires. Construct. Build. Mater. 122, 649–658. https://doi.org/10.1016/j.conbuildmat.2016.06.113
Serjun, V.Z., Mirtic, B., Mladenovic, A., 2013. Evaluation of ladle slag as a potential material for building and civil engineering. Mater. Technol. 47, 543–550.
Sukontasukkul, P., Pongsopha, P., Chindaprasirt, P., Songpiriyakij, S., 2018. Flexural performance and toughness of hybrid steel and polypropylene fibre reinforced geopolymer. Construct. Build. Mater. 161, 37–44. https://doi.org/10.1016/j.conbuildmat.2017.11.122
Turner, L.K., Collins, F.G., 2013. Carbon dioxide equivalent (CO2-e) emissions: a comparison between geopolymer and OPC cement concrete. Construct. Build. Mater. 43, 125–130. https://doi.org/10.1016/j.conbuildmat.2013.01.023
van Deventer, J.S.J., Provis, J.L., Duxson, P., Brice, D.G., 2010. Chemical research and climate change as drivers in the commercial adoption of alkali activated materials. Waste Biomass Valorization 1, 145–155. https://doi.org/10.1007/s12649-010-9015-9
Yan, H., Sun, W., Chen, H., 1999. The effect of silica fume and steel fiber on the dynamic mechanical performance of high-strength concrete. Cement Concr. Res. 29, 423–426. https://doi.org/10.1016/S0008-8846(98)00235-X
Yang, E.-H., Wang, S., Yang, Y., Li, V.C., 2008. Fiber-bridging constitutive law of engineered cementitious composites. J. Adv. Concr. Technol. 6, 181–193. https://doi.org/10.3151/jact.6.181
Yin, S., 2017. Environmental benefits of using recycled PP fibre through a life cycle assessment. In: Yin, S. (Ed.), Development of Recycled Polypropylene Plastic Fibres to Reinforce Concrete. Springer Singapore, Singapore, pp. 103–122. https://doi.org/10.1007/978-981-10-3719-1_6.
Yin, S., Tuladhar, R., Sheehan, M., Combe, M., Collister, T., 2016. A life cycle assessment of recycled polypropylene fibre in concrete footpaths. J. Clean. Prod. 112, 2231–2242. https://doi.org/10.1016/j.jclepro.2015.09.073